Molecular Cancer Therapeutics

Anti-miRNA Oligonucleotide Therapy for Chondrosarcoma

Xiaojuan Sun[1], Yupeng Chen[1,2], Hongchuan Yu[1], Jason T. Machan[1,3,4], Ashna Alladin[1], Jose Ramirez[1], Ross Taliano[5], Jesse Hart[5], Qian Chen[1], and Richard M. Terek[1,6]

Abstract

Chondrosarcoma is a highly aggressive primary malignant bone tumor mostly occurring in adults. There are no effective systemic treatments, and patients with this disease have poor survival. miR-181a is an oncomiR that is overexpressed in high-grade chondrosarcoma and promotes tumor progression. Regulator of G-protein signaling 16 (RGS16) is a target of miR-181a. Inhibition of RGS16 expression by miR-181a enhances CXC chemokine receptor 4 signaling, which in turn increases MMP1 and VEGF expression, angiogenesis, and metastasis. Here, we report the results of systemic treatment with anti-miRNA oligonucleotides (AMO) directed against miR-181a utilizing a nanopiece delivery platform (NPs). NPs were combined with a molecular beacon or anti–miR-181a oligonucleotides and are shown to transfect chondrosarcoma cells *in vitro* and *in vivo*. Intratumoral injection and systemic delivery had similar effects on miR-181a expression in nude mice bearing chondrosarcoma xenografts. Systemic delivery of NPs carrying anti–miR-181a also restored *RGS16* expression, decreased expression of VEGF and MMP1, MMP activity, and tumor volume by 32% at day 38, and prolonged survival from 23% to 45%. In conclusion, these data support that systemic delivery of AMO shows promise for chondrosarcoma treatment.

Introduction

Chondrosarcoma remains the only primary bone cancer without an effective systemic treatment. This sarcoma is highly metastatic. Conventional cytotoxic chemotherapy is not effective, and patients typically succumb to pulmonary metastases (1–3). Another approach for systemic treatment is targeted therapeutics, which have yet to be fully developed. A promising targeted approach is manipulation of misexpressed miRNAs (4). MiRNAs are short, endogenous, noncoding RNAs that negatively regulate gene expression by promoting mRNA degradation or by translational repression through complementarity with sequences in the 3′ untranslated region (5–7). In cancer, miRNAs can function analogous to tumor suppressors or as oncogenes (oncomiRs) when over- or underexpressed, the net effect dependent on the target genes (8, 9). In prior work, we identified miR-181a as an oncomiR that is upregulated by hypoxia in chondrosarcoma, that in turn upregulates VEGF and MMP expression (10, 11). Chondrosarcoma cells transfected with a lentivirus-expressing anti–miR-181a reversed these downstream effects and decreased lung metastatic burden; however, systemic delivery of miRNAs and anti-miRNA oligonucleotides (AMO) remains an unsolved problem (4). There are several types of nanoparticles that can be used for drug and AMO delivery including lipid, polymeric, and metallic nanoparticles (12). One challenge to delivery in chondrosarcoma is the negatively charged proteoglycan-rich extracellular matrix that needs to be penetrated to reach the tumor cells. In order to translate our findings into a potential treatment, we performed systemic treatment with AMO directed against miR-181a delivered with a Nanopiece (NP) platform. NPs are based on a novel biomimetic molecule: 6-amino-fused adenine and thymine, named JBAK (Janus base with Amine or lysine (K) side chain). A JBAK molecule has two components: (1) nucleobases with hydrogen-bond donors and acceptors on two faces respectively, and (2) a hydrophilic side chain containing amine or lysine. We used the lysine side chain in these experiments. With this design, two faces of a Janus Base are complementary to each other, and six JBAK molecules form a disc which further self-assembles into a hydrophobic tubular backbone with the positively charged amine or lysine containing side chains remaining on the surface of this tubular structure, thus forming a rosette nanotube: Janus Base Nanotube (JBNT; ref. 13). Through positive–negative charge interaction, and when combined with nucleic acid therapeutics such as siRNA or AMO, and after treatment with ultrasonic energy, they form NPs, with a size of 120 × 20 nmol/L (14). NPs are nontoxic and can penetrate negatively charged cartilaginous matrix, which is also found in chondrosarcoma (15–18). The pathway and NP delivery of AMO are diagrammed in Fig. 1A.

Here, we demonstrate for the first time that (1) NPs can deliver nucleotide sequences intracellularly to human tumor cells *in vitro* and *in vivo*, and (2) NPs-carrying AMOs administered systemically

[1]Department of Orthopaedics, Warren Alpert Medical School of Brown University and Rhode Island Hospital, Providence, Rhode Island. [2]Department of Biomedical Engineering, University of Connecticut, Storrs, Connecticut. [3]Lifespan Biostatistics Core, Lifespan Hospital System, Providence, Rhode Island. [4]Department of Surgery, Warren Alpert Medical School of Brown University and Rhode Island Hospital, Providence, Rhode Island. [5]Department of Pathology, Warren Alpert Medical School of Brown University and Rhode Island Hospital, Providence, Rhode Island. [6]Providence Veterans Administration Medical Center, Providence, Rhode Island.

Note: Supplementary data for this article are available at Molecular Cancer Therapeutics Online (http://mct.aacrjournals.org/).

Corresponding Author: Richard M. Terek, Warren Alpert Medical School of Brown University and Rhode Island Hospital, 1 Hoppin St, Providence, RI 02903. Phone: 401-457-1555; Fax: 401-831-8992; E-mail: Richard_Terek@Brown.edu

Mol Cancer Ther 2019;18:2021–9

doi: 10.1158/1535-7163.MCT-18-1020

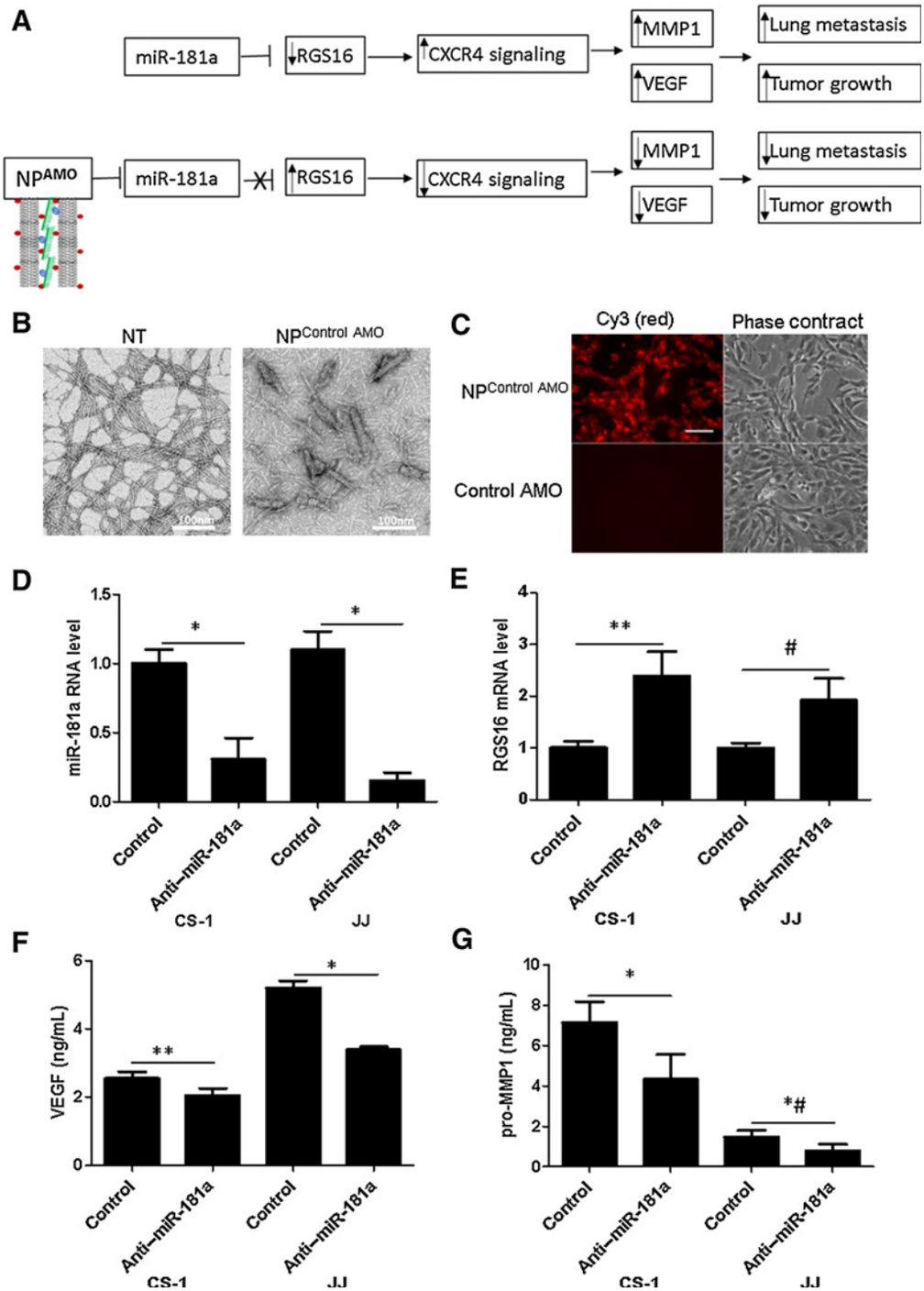

Figure 1.

Nanopiece characterization and transfection of chondrosarcoma cells. **A,** (Top) Pathway by which endogenous overexpression of miR-181a enhances CXCR4 signaling via inhibition of RGS16 is shown. CXCR signaling increases MMP1 and VEGF expression, leading to tumor progression. (Bottom) Schematic of anti–miR-181a (AMO) delivery by NP to chondrosarcoma cells and reversal of enhanced CXCR4 signaling, resulting in inhibition of tumor progression. Red indicates positive charges on NP, and blue indicates negative charges on AMO (green). **B,** Transmission electron microscopy of JBNT (left) and Nanopieces combined with AMO (right). After combination of JBNT with AMO and ultrasonic treatment, the size was reduced. Scale bar, 100 nm. **C,** Transfection with NP was first evaluated using Cy3-labeled control AMO. Representative images 1 day after incubation with $NP^{Control\text{-}Cy3}$ (top) or Control-Cy3 alone (bottom). Scale bar, 50 μm. **D,** miR-181a expression was evaluated with real-time PCR 2 days after incubation with $NP^{anti\text{-}miR\text{-}181a}$ or control (*, $P < 0.001$, $n = 3$). **E,** *RGS16* mRNA was quantitated with real-time PCR after transfection with $NP^{anti\text{-}miR\text{-}181a}$ or control (**, $P < 0.01$; #, $P < 0.05$; $n = 3$). VEGF (**F**) and pro-MMP1 (**G**) were quantified in CM with ELISA after transfection with $NP^{anti\text{-}miR\text{-}181a}$ or control (*, $P < 0.001$; **, $P < 0.01$; #, $P < 0.05$; $n = 4$).

inhibit expression of an oncogenic miRNA, restore expression of *RGS16*, and have a favorable effect on tumor-related parameters in a preclinical model.

Materials and Methods

Cell lines and cell culture

Human chondrosarcoma cell lines CS-1 (a gift from Dr. Francis Hornicek, Harvard Medical School, Boston, MA) and JJ (a gift from Dr. Joel Block, Rush Medical School, Chicago, IL) were cultured with 10% FBS in a humidified incubator (NuAire Inc.) under 5% CO_2 and normoxia (ambient oxygen) as previously described (11, 18, 19). CS-1 was derived from grade III and JJ from grade II human chondrosarcomas, respectively; both metastasize in a xenograft mouse model. (11, 19, 20). The CS-1 cell line was authenticated using short tandem repeat (STR) profiling (ATCC) in September 2012, matched the STS profiling performed by the source laboratory in 2011, and there were no other matches in the ATCC data base. JJ was authenticated using STR profiling on the source cell line in 1999, 2007, and repeated in 2012. There is 94% similarity between the different time points, the cells are human, and there are no matches with any cell lines in the ATCC database. Frozen aliquots of cells were used for this study.

Molecular beacon; oligonucleotides

The sequence of the molecular beacon for Human GAPDH was 5′-Alexia647- CGACGGAGTCCTTCCACGATACCACGTCG-BHQ3a-3′ (Eurofins Genomics; ref. 21).

mirVana miRNA inhibitor specific for human miR-181a and mirVana miRNA inhibitor Negative Control #1 were purchased (Thermo Fisher Scientific).

Preparation of NPs

The Janus base nanotubes were synthesized as previously described and dissolved in water to a 1 mg/mL solution (14). For cell culture experiments, NPs were generated by mixing 2 μL of AMO (50 μmol/L) with 30 μL of nanotube (1 mg/mL), followed by sonication for 2.5 minutes at 22 Watts/cm^2 (Q700 Sonicator, Qsonica). The assembled NPs were mixed with 1 mL of cell culture medium and incubated with cells for 48 hours without any transfection reagents. For animal experiments, each dose of NPs was generated by mixing 7 μL of AMO (50 μmol/L) with 105 μL of JBNT (1 mg/mL), followed by sonication for 2.5 minutes. Note that 45.5 μL PEG 400 (Sigma) and 25.2 μL glucose solution (55% wt./vol; Sigma) were added to the NP solution (total volume 182.7 μL). Each control dose contained the same components, except for the 7 μL of control anti-miR (50 μmol/L).

NPs were also generated for tracer experiments using a molecular beacon for GAPDH. Twenty microliter of 20 nmol/L of GAPDH molecular beacon and 60 μL of JBNT (1mg/mL) were mixed and diluted with water to 100 μL; then sonicated and mixed with 26 μL PEG 400 (Sigma) and 14.4 μL glucose solution (55% wt./vol; Sigma); and final volume was 140.4 μL. For transmission electron microscopy studies, a 15 μL sample of nanotube or NP solution was mounted on a carbon-coated copper grid (EM Sciences) and stained using a droplet of 2% aqueous uranyl acetate for 30 seconds. Excess staining agent was blotted with filter paper, and the grid was dried at room temperature. The images were obtained on a MorgagniTM 268 microscope (FEI) at a magnification of 20,000 to 140,000 under an acceleration voltage of 80 kV. A toxicity study has been conducted with NPs (15, 22). They did not cause apoptosis *in vitro* or organ toxicity *in vivo* at the concentrations and doses used in this study.

RNA isolation

Total RNA including miRNA was extracted from CS-1 and JJ cells and xenograft tumors using miRNeasy Mini Kit (Qiagen). The concentration and quality of total RNA were determined with a NanoDrop 2000C spectrophotometer (Thermo Fisher Scientific). Samples with purity of 1.8-2 and integrity over 1.6 were used for analysis of miRNA expression.

MiRNA expression

Total RNA was reverse transcribed using the miScript Reverse Transcription Kit (Qiagen), and quantification of the ubiquitously expressed miRNA *U17a* was used as an internal control. A reaction mixture (20 μL) containing the SYBR Green Master Mix (Qiagen), 2 ng of cDNA template plus miScript Universal primer and miScript Primer Assay (miR-specific primer for miR-181a) in a 96-well plate was used for real-time PCR using miScript SYBR Green PCR kit (Qiagen). The reactions were done in triplicate on the DNA engine CFX96 Real-time PCR amplification system (Bio-Rad). PCR conditions were as follows: an initial step at 95°C for 10 minutes, followed by 40 cycles of amplification at 94°C for 10 seconds, 55°C for 30 seconds, and then 70°C for 30 seconds.

mRNA expression

RGS16 and MMP1 mRNA were quantified using the Reverse Transcription System (Bio-Rad) followed by real-time PCR with SYBR Green Master Mix (Qiagen). B2M was used as the internal control (23, 24). The primers for *RGS16*, *MMP1*, and *B2M* have been previously published (25–27). The comparative threshold cycle (Ct) method, i.e., $2^{-\Delta\Delta Ct}$ method was used for the calculation of fold amplification (28). The data analysis was performed as previously described (26, 28).

ELISA assay

Lysates from conditioned media (CM) from cultured cells and homogenized xenograft tumors were used for ELISA assay. Cells were cultured for 1 day, then the medium was changed to 1% FBS O/N, and the CM were collected to measure VEGF and pro-MMP1 concentration (R&D system; refs. 20, 25). Each sample was measured in duplicate, and each experiment was repeated at least 3 times. VEGF and MMP1 were normalized to the lysate protein concentration as determined by Quick Start Brandford protein assay (Bio-Rad).

Mouse model, bioimaging, tumor growth, and metastasis analysis

Xenograft tumors in nude mice were generated as previously described (20). Briefly, 1×10^6 CS-1 cells in 100 μL culture medium mixed with 300 μL Matrigel (BD Biosciences) were injected s.c. in the back of nude mice (nu/nu 6–8-week-old, female, Charles River Laboratory).

In vivo bioimaging was performed with Fluorescence Molecular Tomography (FMT, PerkinElmer) 2 weeks after the start of treatment. Twenty-four hours before imaging, mice were injected via tail vein with 2 nmol MMPSense 680 and AngioSense 750 (PerkinElmer). Mice were anesthetized with ketamine (i.p.) during FMT imaging. FMT is acquired with a continuous wave-type scanner capable of acquiring transillumination, reflectance, and absorption data at 680 nm excitation and 700 nm emission or

750 nm excitation and 780 nm emission (PerkinElmer). AngioSense and MMPSense content in xenograft tumors was determined by region-of-interest analysis as previously described (20).

Mice were treated with seven i.v. injections of $NP^{antimiR\text{-}181a}$ or control over a 3-week period starting 2 weeks after implantation of chondrosarcoma cells. Tumors and lungs were harvested at 6 weeks after implantation of tumor cells or sooner if required by our Institutional Animal Care and Use Committee (IACUC) protocol as determined by veterinary staff, who were blinded to treatment group.

Primary tumor analysis

Tumor size was measured throughout the experiment, and tumor weight was determined at the time of excision. Tumor volume was calculated by the formula $V = HWL \times 0.52$, where H, W, and L are the height, width, and length of the tumor, respectively. Part of the excised tumor was fixed in 10% formalin overnight, paraffin embedded, and used for hematoxylin and eosin (H&E) staining. Some of the tumor was stored in RNA later for RNA extraction or lysis buffer for protein extraction.

Metastasis analysis

The number of mice in each group with metastases was compared with the χ^2 test. Lung metastatic burden was quantified as previously described (29). Briefly, lungs were analyzed with microscopy after fixation in 10% formalin. Transverse sections were made at 350 μm intervals yielding approximately 40 sections per lung. H&E-stained slides were scanned using the Philips Ultra Fast Scanner (Philips), and extracted images were analyzed using Image Pro image analysis software (Media Cybernetics). Lung tissue area was measured using an automated algorithm. To correct for variation in bronchus dilation, subtraction of dead space of the larger airways and vascular spaces was included as a component of the algorithm. Measurement of the area of the metastases, as well as exclusion of nonpulmonary tissues, was performed manually. Metastatic burden was quantified as the proportion of sections with metastases, the total number of nodules per lung, and the total area of the nodules normalized to the total lung area. The average area fraction is an accepted estimate of the volume fraction (30).

Study approval

All animal studies were approved by the IACUC at Rhode Island Hospital and were carried out in accordance with the National Institutes of Health Guide for the Care and Use of Laboratory Animals (eighth edition).

Statistical analysis

All experiments were repeated at least 3 times. Experiments with two groups were analyzed with the Student t test unless otherwise specified (Mann–Whitney U test was used for data not normally distributed). Experiments with three or more groups were compared with one-way ANOVA, followed by the Student t test with Bonferroni correction for individual comparisons. Data are presented as mean ± SD.

Generalized linear models were used to compare mice who received anti–miR-181a with control anti-miR. The negative binomial distribution was used for analysis of MMPSense and AngioSense probe content, tumor weight, and total number of nodules per lung. The negative binomial distribution is positively skewed with distinct parameters for central tendency and variance, as well as having no negative values. These variables are each positively skewed and cannot be negative. This makes the negative binomial distribution superior to the Gaussian distribution for these measures. The binomial distribution was used for analysis of the proportion of sections with metastases and the normalized areas of nodules. The binomial distribution represents a distribution with parameters for a rate of event within a number of opportunities which more appropriately bounds the statistical model to fall between 0 and 100, as well as appropriately skewing the distribution toward 50% as estimates approach the bounds. Classical sandwich estimation was used to adjust for any model misspecification. The Wilcoxon weighted χ^2 test was used to compare Kaplan–Meier survival functions of times-to-event outcomes. Time was measured in days from tumor implantation. Statistical analysis was performed with SAS version 9.4 (The SAS Institute) and Prism version 5.04 (GraphPad). The null hypothesis of no difference was rejected at a significance level of 5%.

Results

Nanopiece delivery of nucleotides

JBNT (Fig. 1B, left) were mixed with AMO, and NPs (Fig. 1B, right) were created as described in the Materials and Methods section. Transmission electron microscopy was used to analyze JBNT and NPs. The JBNT were too long and intertwined to measure, whereas the average size of NPs is112.3 nm ± 48.6 nm in length and 17.3 nm ± 9.5 nm in width (Fig. 1B, right). As a first step to test if NPs can deliver AMO to chondrosarcoma cells, we incubated CS-1 cells with Cy3-labeled control AMO alone or with NP^{AMO}. Intracellular fluorescence is only seen with NP^{AMO} (Fig. 1C, top left).and not with AMO alone (Fig. 1C, bottom left). To test if miRNA knockdown could be achieved with NP delivery, CS-1 and JJ cells were incubated with $NP^{anti\text{-}miR\text{-}181a}$. $NP^{anti\text{-}miR\text{-}181a}$ reduced expression of miR-181a (Fig. 1D), restored expression of *RGS16* (Fig. 1E), and reduced further downstream targets VEGF and MMP1 (Fig. 1F and G) compared with $NP^{control\ AMO}$.

To determine whether NPs can deliver nucleotide sequences intracellularly *in vivo*, a molecular beacon for *GAPDH* (mb*GAPDH*) alone or carried by NPs was administered by tail vein injection to mice bearing xenograft tumors. The molecular beacon contains a nucleotide sequence complementary to a specific mRNA target flanked by a quencher and a fluorescent probe, which fluoresces only after binding the intracellular target mRNA, in this case a house keeping gene *GAPDH*. Tumor fluorescence was only observed when the $NP^{mbGAPDH}$ was used (Fig. 2). Fluorescence is also seen in the spleen and liver in both the control and experimental groups, indicating that the molecular beacon can be taken up by the mononuclear phagocyte system directly. In contrast, mb*GAPDH* signals were only seen in the tumor when NPs were used for delivery, indicating NPs were required for beacon delivery to the tumor.

We then compared local tumor injection with systemic injection of $NP^{anti\text{-}miR\text{-}181a}$. miR-181a expression was reduced by 52% when xenograft tumors were injected with $NP^{anti\text{-}miR\text{-}181a}$ (Fig. 3A). Similarly, when $NP^{\ antagomir\text{-}181a}$ (at doses of 0.35 and 0.7 nmol of anti-miR) were administered systemically, miR-181a was reduced to 44.7% and 32.2% of control, respectively (Fig. 3B). In subsequent *in vivo* experiments, the lower dose was used for tail vein injections because of limited availability of JBNT.

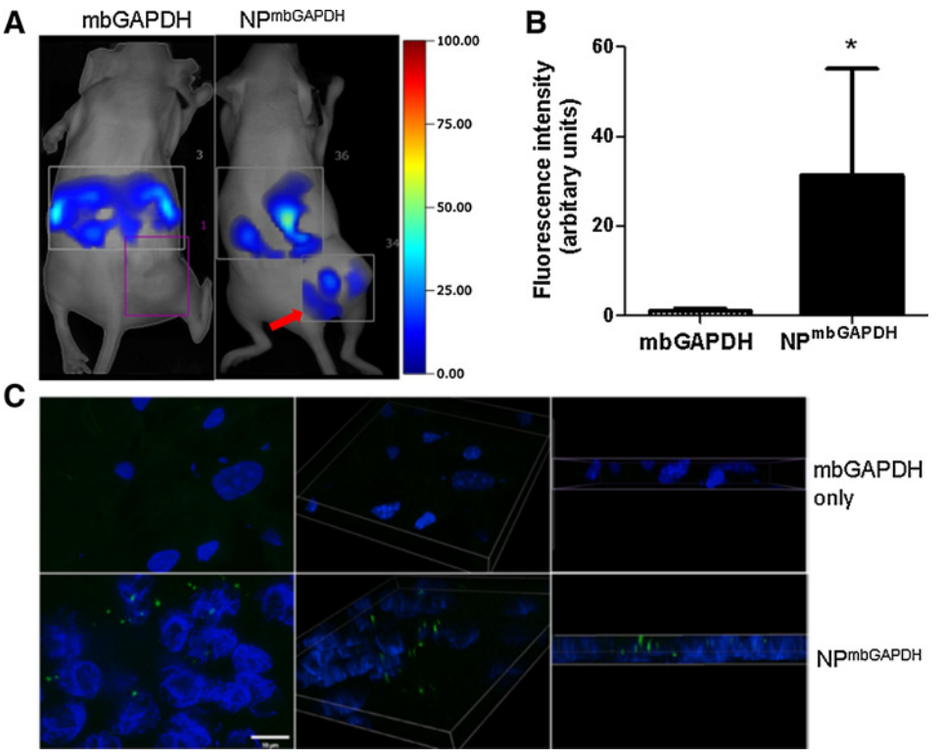

Figure 2.
Nanopieces transfect xenograft tumors with molecular beacon. Mice bearing xenograft tumors were administered mb*GAPDH* alone or with NP ($NP^{mbGAPDH}$). **A,** FMT images 1 day later show tumor fluorescence only after combination of beacon and NP (arrow). **B,** Quantification of fluorescent intensity in xenograft tumors ($n = 4, 5$; *, $P < 0.02$, Mann–Whitney *U*). **C,** Confocal microscopy of xenograft tumor sections demonstrates intracellular fluorescence after $NP^{mbGAPDH}$ (bottom), but not with mb*GAPDH* alone, top). Size bar, 10 μm.

Nanopiece/anti–miR-181a inhibits miR-181a expression, tumor growth, MMP1 expression, and activity, and increases survival in a xenograft model

A mouse xenograft chondrosarcoma model was used to assess whether the NP platform could be used for delivery of nucleotide-based therapy. MiR-181a was reduced to 46% of control in the xenograft tumors (Fig. 4A). In prior work, we found that *RGS16* is a direct target of miR-181a, and that diminished expression of RGS16 enhances CXCR4 signaling, which culminates in MMP1 and VEGF expression (11). In the treated mice, *RGS16* mRNA expression was restored and *MMP1* mRNA expression decreased (Fig. 4B), and both MMP1 and VEGF protein content decreased (Fig. 4C). FMT *in vivo* imaging indicated decreased MMP activity in the tumors (Fig. 4D); angiogenesis was not significantly affected (Fig. 4E). Tumor weight was reduced by 25% (Fig. 4F) and tumor volume by 32% at day 38 (Fig. 4G). More importantly, survival as measured by days to forced euthanasia was almost doubled at day 48 in the treatment group (23% vs. 45%; Fig. 4H). There were fewer mice with metastases (11/13 vs. 5/11, $P < 0.04$) and a decrease in the proportion of lung sections with tumor (0.154 vs. 0.048; Fig. 4I and J). The number of metastatic nodules per lung (8.4 vs. 2.4) and normalized area of nodules per lung (0.12 vs. 0.04) were not different (Supplementary Fig. S1). Taken together, the results indicate that the systemic delivery of $NP^{anti\text{-}miR\text{-}181a}$ inhibited miR-181a overexpression, downstream targets, and tumor progression.

Discussion

We previously showed as proof of principle that miR-181a is a therapeutic target by pretransfection of CS-1 cells with a lentivirus expressing anti–miR-181a before implantation into mice (11). This reduced miR-181a in xenograft tumors and inhibited CXCR4 signaling and tumor progression (11). In this study, we used a nonviral, biomimetic nanoparticle to deliver AMOs. Essentially all the effects achieved with the lentivirus construct were

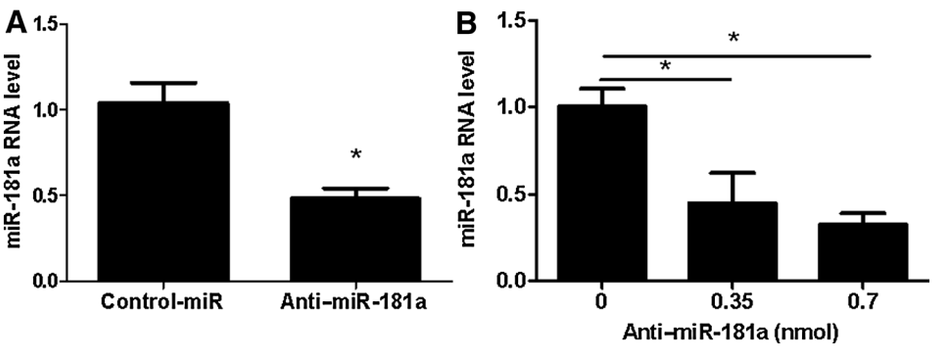

Figure 3.
Both local and systemic delivery of $NP^{anti\text{-}miR\text{-}181a}$ reduce miR-181a expression in xenograft tumors. **A,** miR-181a in xenograft tumors was quantified with real-time PCR 2 days after local injection of $NP^{control\ AMO}$ or $NP^{-anti\text{-}miR\text{-}181a}$ (0.35 nmol) into xenograft tumor 2 times/week for 2 weeks. *, $P < 0.001$, $n = 8$. **B,** miR-181a level in xenograft tumors 2 days after systemic administration of three doses of $NP^{control\ AMO}$ or $NP^{-anti\text{-}miR\text{-}181a}$ (*, $P < 0.001$, $n = 3$/group).

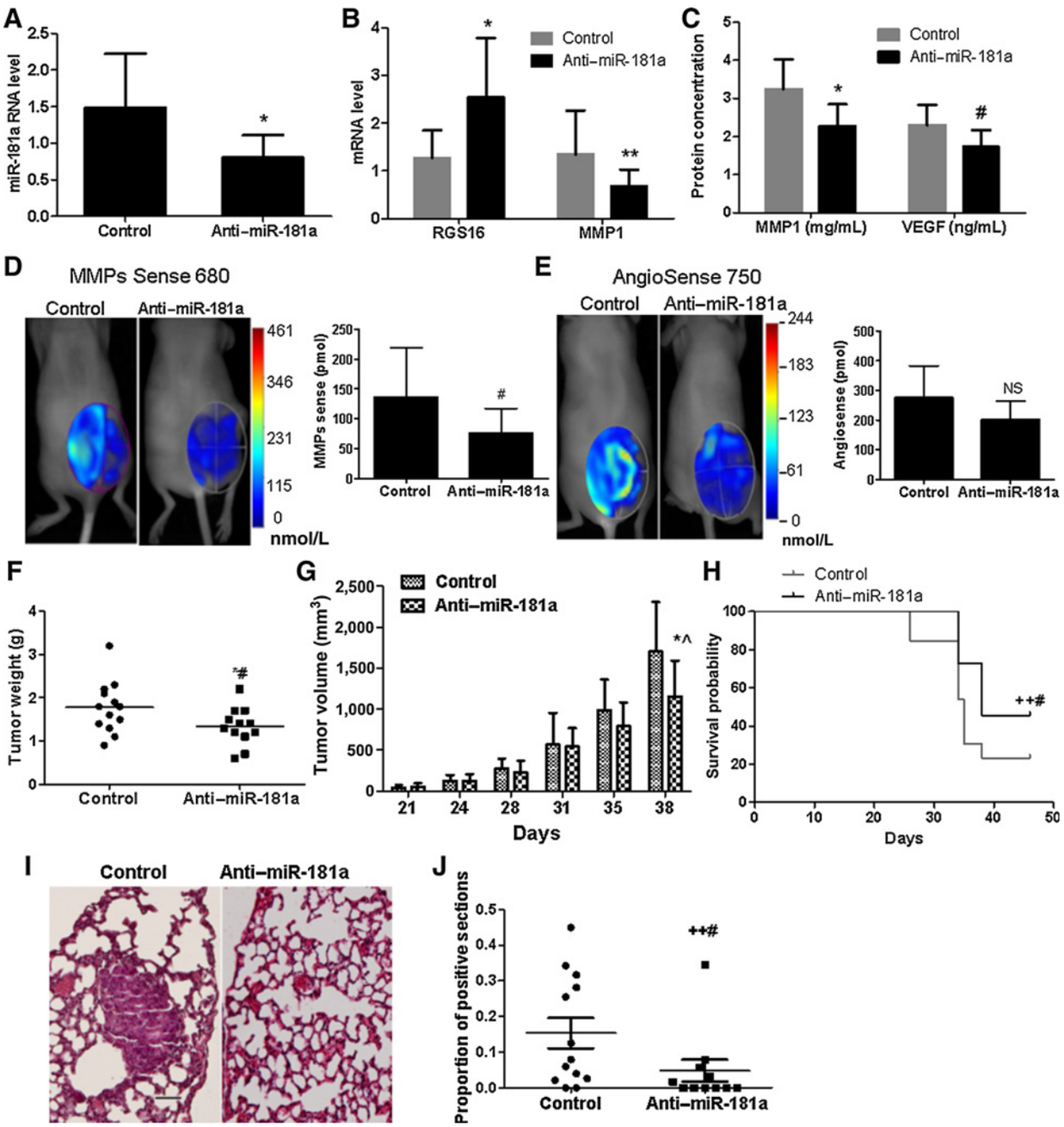

Figure 4.

Systemic NP$^{\text{anti-miR-181a}}$ restores *RGS16* expression and inhibits chondrosarcoma growth. Mice bearing xenograft tumors were treated with seven i.v. injections of NP$^{\text{control AMO}}$ or NP$^{\text{anti-miR-181a}}$ over a 3-week period starting 2 weeks after implantation of chondrosarcoma cells. **A,** qRT-PCR quantification of miR-181a in xenograft tumors (*, $P < 0.01$, $n = 11$/group Mann–Whitney *U*). **B,** qRT-PCR quantification of *RGS16* and *MMP1* mRNA level (*, $P < 0.01$, Mann–Whitney U; **, $P < 0.04$, $n = 11$/group). **C,** MMP1 and VEGF protein expression in xenograft tumors (*, $P < 0.01$; #, $P < 0.03$, $n = 8$/group). **D** and **E,** FMT imaging with MMPSense and AngioSense ($n = 13, 11$, #, $P < 0.03$; NS, $P < 0.06$). **F,** Final tumor weight (*#, $P < 0.05$; $n = 13, 11$). **G,** Tumor volume (*^, $P < 0.02$, $n = 13, 11$). **H,** Kaplan–Meier survival curves ($^{++\#}$, $P = 0.05$, $n = 13,11$). **I,** Representative H&E sections of lungs from control and treatment groups. Metastatic burden (**J**) proportion of positive sections ($^{++\#}$, $P = 0.05$, $n = 13, 11$).

recapitulated here, albeit to a lesser degree, suggesting that our NP delivery platform is successful for delivering AMOs in a preclinical model. In addition, survival was improved in the current study. Most if not all advanced cancers are incurable, and current targeted therapies aim to slow tumor progression and improve quality of life.

In prior work, we determined that one mechanism of miR-181a overexpression that results in tumor metastasis is inhibition of

RGS16 (11). RGS proteins are critical modulators of signal transduction pathways in normal physiology and in cancer. Diminished RGS16 leads to progression of several types of carcinoma as well as chondrosarcoma (11, 31–33). RGS16 is an innate negative regulator of CXCR4 signaling, so that inhibiting expression of an inhibitor results in gain of function in CXCR4 signaling. CXCR4 expression is increased in chondrosarcoma and mediates cell motility and metastasis (20, 25). CXCR4 signaling activity is enhanced by inhibition of RGS16, which results from increased miR-181a expression. Increased miR-181a and CXCR4 expression are at least partially a result of hypoxia (11, 25). Increased CXCR4 signaling increases MMP1 and VEGF expression, invasion, and metastases (10, 11, 20, 25). Angiogenesis and invasion are partially mediated by VEGF and MMP, are enhanced by hypoxia, and are critical features of malignancy (34). Our work has focused on understanding these aspects of tumor biology and developing targeted therapeutics. Based on the effects of knocking down miR-181a expression with a lentivirus construct on RGS16 expression and inhibiting metastatic pathways, we postulated that antagomir-based therapy might be efficacious and potentially better than inhibition of CXCR4 signaling with the drug AMD3100 (11, 20). The advantage of the AMO approach is that multiple, partially redundant signaling pathways related to tumor progression may be targeted: one reason AMO strategies are under clinical development (35, 36). Another potential advantage of NPs is that they can be loaded with combinations of shRNA, RNAi, AMO, and drugs (37, 38). In this study, we demonstrated that an AMO strategy can inhibit expression of an oncomiR (miR-181a), restore *RGS16* expression (Fig. 4B), inhibit tumor progression, and prolong survival. Therefore, NP^{AMO} may be an effective treatment for chondrosarcoma, other tumor types, and diseases of cartilage in which RGS16 and other miR-181a targets are overexpressed. The twice-weekly systemic administration that was used in this study could be reasonably utilized in the clinic. In comparison with AMD3100, which was administered b.i.d for 6 weeks, and continuous knockdown of miR-181a with the lentivirus construct, the effects on tumor growth and metastases were, as expected, less in this study.

There are several technical challenges in the use of nanoparticles in clinical applications. One challenge is penetration of tumor tissue with therapeutics. Similar to chondrocytes, chondrosarcoma cells produce a cartilaginous matrix which is composed of type II collagen and proteoglycans. Proteoglycans are negatively charged, and the pore size in cartilaginous matrix ranges from 6 to 100 nm (39). These properties may limit anticancer drug diffusion and infiltration (40). An important property of NPs is their positive surface charge. After ultrasonic treatment, NP^{AMO} are rod shaped and have a diameter of only 17 nm, much smaller than conventional spherical nanoparticles which have diameters typically larger than 60 nm (Fig. 1A; refs. 40–43). The positive charge and small size are advantageous in penetration of the matrix, and we have also shown that NPs can penetrate articular cartilage matrix (16).

Toxicity is of concern with clinical use of nanoparticles. Viruses can cause inactivating immune responses and have mutagenic risks (44). Lipid nanoparticles have been used for tumor delivery of drugs and RNA therapeutics. However, a recent phase I clinical trial for solid tumor treatment utilizing MRX34, a liposomal miR-34a mimic, was terminated due to unexplained immune-related serious adverse events. It is not clear if the toxicity was related to miR-34a mimic or the liposomal nanoparticles (45). An additional advantage of NPs is their low toxicity and better safety profile compared with viruses or lipid-based nanoparticles, because they are assembled from nucleotide-derived JBAK that mimic natural biological molecules (16).

There are some limitations to our study. We did not attempt to target NPs to the tumor cells but relied on increased vascular permeability characteristic of tumor vessels. Nontargeted NP therapy is similar to the delivery of chemotherapy in other cancers. We did not determine the mechanism of NP uptake by tumor cells, although we think it may be mediated by endocytosis.

Although we identified *RGS16* as one relevant target of miR-181a, in this study, we did not attempt to validate other targets of miR-181a. We have, however, identified additional candidate targets by comparing CS-1 cells transfected with control miR or anti–miR-181a with gene array analysis. These data have been deposited in NCBI's Gene Expression Omnibus and are accessible through GEO Series accession number GSE70065 (https://www.ncbi.nlm.nih.gov/geo/query/acc.cgi?acc=GSE70065; ref. 46). We used a subcutaneous xenograft model rather than an orthotopic model. An advantage of the subcutaneous model is more consistent tumor growth kinetics, more precise measurement of tumor growth, and better *in vivo* bioimaging. An advantage of the orthotopic model is tumor–stromal cell interaction, which can facilitate tumor progression. A disadvantage is the functional impairment and distress to the animals which can limit the length of the experiments and survival analysis.

In conclusion, our results confirm that miR-181a is an oncomir, whose knockdown via systemic delivery restores expression of *RGS16* and inhibits tumor progression. Further optimization of formulation, targeting, dosing, and loading of NPs with AMO or combinations of different miRNAs, AMOs, and drugs may yield better results. The NP platform can be used for experimental delivery of nucleotide-based therapeutics and AMO therapy that may have potential for cancer treatment.

Disclosure of Potential Conflicts of Interest

Y. Chen has an ownership interest (including patents) in, and has an unpaid consultant/advisory board relationship with, NanoDe Therapeutics. Q. Chen has an ownership interest (including patents) in NanoDe Therapeutics Inc. No potential conflicts of interest were disclosed by the other authors.

Authors' Contributions

Conception and design: X. Sun, Y. Chen, J.T. Machan, Q. Chen, R.M. Terek
Development of methodology: X. Sun, Y. Chen, H. Yu, J.T. Machan, Q. Chen, R.M. Terek
Acquisition of data (provided animals, acquired and managed patients, provided facilities, etc.): Y. Chen, H. Yu, A. Alladin, J. Ramirez
Analysis and interpretation of data (e.g., statistical analysis, biostatistics, computational analysis): X. Sun, Y. Chen, J.T. Machan, A. Alladin, J. Ramirez, R. Taliano, J. Hart, Q. Chen, R.M. Terek
Writing, review, and/or revision of the manuscript: X. Sun, Y. Chen, J.T. Machan, R. Taliano, Q. Chen, R.M. Terek
Administrative, technical, or material support (i.e., reporting or organizing data, constructing databases): Y. Chen, H. Yu, J.T. Machan, A. Alladin
Study supervision: Y. Chen, Q. Chen, R.M. Terek

Acknowledgments

The authors thank Dr. Francis Hornicek for the CS-1 cell line and Dr. Joel Block for the JJ cell line.

One or more of the authors have received funding from the NIH and from the National Institute of General Medical Sciences, a component of NIH: Y. Chen (grants 1R01AR072027-01, 1R03AR069383-01 and NSF Career Award 1653702), H. Yu (grant 20164374 from Rhode Island Foundation), Q. Chen

(grants P30GM122732 and P20GM104937), and R.M. Terek (grant 1R01CA166089).

The costs of publication of this article were defrayed in part by the payment of page charges. This article must therefore be hereby marked *advertisement* in accordance with 18 U.S.C. Section 1734 solely to indicate this fact.

Received September 11, 2018; revised May 10, 2019; accepted July 19, 2019; published first July 24, 2019.

References

1. Soderstrom M, Ekfors TO, Bohling TO, Teppo LH, Vuorio EI, Aro HT. No improvement in the overall survival of 194 patients with chondrosarcoma in Finland in 1971-1990. Acta Orthop Scand 2003;74:344–50.
2. Giuffrida AY, Burgueno JE, Koniaris LG, Gutierrez JC, Duncan R, Scully SP. Chondrosarcoma in the United States (1973 to 2003): an analysis of 2890 cases from the SEER database. J Bone Joint Surg Am 2009;91: 1063–72.
3. Nazeri E, Gouran SM, Majidzadeh A, Esmaeili R. Chondrosarcoma: an overview of clinical behavior, molecular mechanisms mediated drug resistance and potential therapeutic targets. Crit Rev Oncol Hematol 2018;131:102–9.
4. Baumann V, Winkler J. miRNA-based therapies: strategies and delivery platforms for oligonucleotide and non-oligonucleotide agents. Future Med Chem 2014;6:1967–84.
5. Fire A, Xu S, Montgomery MK, Kostas SA, Driver SE, Mello CC. Potent and specific genetic interference by double-stranded RNA in Caenorhabditis elegans. Nature 1998;391:806–11.
6. Grishok A, Pasquinelli AE, Conte D, Li N, Parrish S, Ha I, et al. Genes and mechanisms related to RNA interference regulate expression of the small temporal RNAs that control C. elegans developmental timing. Cell 2001; 106:23–34.
7. Seydoux G, Mello CC, Pettitt J, Wood WB, Priess JR, Fire A. Repression of gene expression in the embryonic germ lineage of C. elegans. Nature 1996; 382:713–6.
8. Dalmay T, Edwards DR.MicroRNAs and the hallmarks of cancer. Oncogene 2006;25:6170–5.
9. Rupaimoole R, Calin GA, Lopez-Berestein G, Sood AK. miRNA deregulation in cancer cells and the tumor microenvironment. Cancer Discov 2016; 6:235–46.
10. Sun X, Wei L, Chen Q, Terek RM. MicroRNA regulates vascular endothelial growth factor expression in chondrosarcoma cells. Clin Orthop Relat Res 2015;473:907–13. doi: 10.1007/s11999-014-3842-0.
11. Sun X, Charbonneau C, Wei L, Chen Q, Terek RM. miR-181a targets RGS16 to promote chondrosarcoma growth, angiogenesis, and metastasis. Mol Cancer Res 2015;13:1347–57.
12. Palazzolo S, Bayda S, Hadla M, Caligiuri I, Corona G, Toffoli G, et al. The clinical translation of organic nanomaterials for cancer therapy: a focus on polymeric nanoparticles, micelles, liposomes and exosomes. Curr Med Chem 2018;25:4224–68.
13. Fenniri H, Deng BL, Ribbe AE, Hallenga K, Jacob J, Thiyagarajan P. Entropically driven self-assembly of multichannel rosette nanotubes. Proc Natl Acad Sci U S A 2002;99:6487–92.
14. Chen Q, Yu H, Chen Y, inventors; Nanomaterials Compositions, Synthesis, and Assembly.WO2016081522. 2016 May 16.
15. Journeay WS, Suri SS, Moralez JG, Fenniri H, Singh B. Rosette nanotubes show low acute pulmonary toxicity in vivo. Int J Nanomedicine 2008;3: 373–83.
16. Vorrius B, Yu H, Guo L, Chen Q, Chen Y. Nanopiece: a nontoxic RNA delivery vehicle into articular cartilage and joint tissues. Trans Orthop Res Soc 2016;41:15.
17. Chen. Nanopiece delivery of IL-1R siRNA into cartilage to treat post-traumatic osteoarthritis. Trans Orthop Res Soc 2016;41:1353.
18. Block JA, Inerot SE, Gitelis S, Kimura JH. Synthesis of chondrocytic keratan sulphate-containing proteoglycans by human chondrosarcoma cells in long-term cell culture. J Bone Joint Surg Am 1991;73:647–58.
19. Susa M, Morii T, Yabe H, Horiuchi K, Toyama Y, Weissbach L, et al. Alendronate inhibits growth of high-grade chondrosarcoma cells. Anticancer Res 2009;29:1879–88.
20. Sun X, Charbonneau C, Wei L, Yang W, Chen Q, Terek RM. CXCR4-targeted therapy inhibits VEGF expression and chondrosarcoma angiogenesis and metastasis. Mol Cancer Ther 2013;12:1163–70.
21. Desai HV, Voruganti IS, Jayasuriya C, Chen Q, Darling EM. Live-cell, temporal gene expression analysis of osteogenic differentiation in adipose-derived stem cells. Tissue Eng Part A 2014;20:899–907.
22. B.Vorrius HYLGWLQCaYC. Nanopiece: a nontoxic RNA delivery vehicle into articular cartilage and joint tissues. Trans Orthop Res Soc 2016;41:15.
23. Asur R, Balasubramaniam M, Marples B, Thomas RA, Tucker JD. Bystander effects induced by chemicals and ionizing radiation: evaluation of changes in gene expression of downstream MAPK targets. Mutagenesis 2010;25: 271–9.
24. Banda M, Bommineni A, Thomas RA, Luckinbill LS, Tucker JD. Evaluation and validation of housekeeping genes in response to ionizing radiation and chemical exposure for normalizing RNA expression in real-time PCR. Mutat Res 2008;649:126–34.
25. Sun X, Wei L, Chen Q, Terek RM. CXCR4/SDF1 mediate hypoxia induced chondrosarcoma cell invasion through ERK signaling and increased MMP1 expression. Mol Cancer 2010;9:17.
26. Sun X, Wei L, Chen Q, Terek RM. HDAC4 represses vascular endothelial growth factor expression in chondrosarcoma by modulating RUNX2 activity. J Biol Chem 2009;284:21881–90.
27. Berthebaud M, Riviere C, Jarrier P, Foudi A, Zhang Y, Compagno D, et al. RGS16 is a negative regulator of SDF-1-CXCR4 signaling in megakaryocytes. Blood 2005;106:2962–8.
28. Livak KJ, Schmittgen TD.Analysis of relative gene expression data using real-time quantitative PCR and the 2(-Delta Delta C(T)) method. Methods 2001;25:402–8.
29. Cisowski J, Sayin VI, Liu M, Karlsson C, Bergo MO. Oncogene-induced senescence underlies the mutual exclusive nature of oncogenic KRAS and BRAF. Oncogene 2016;35:1328–33.
30. Aherne WA, Dunhill MS. Morphometry. London: Edward Arnold; 1982. p. 37.
31. Kim JH, Lee JY, Lee KT, Lee JK, Lee KH, Jang KT, et al. RGS16 and FosB underexpressed in pancreatic cancer with lymph node metastasis promote tumor progression. Tumour Biol 2010;31:541–8.
32. Liang G, Bansal G, Xie Z, Druey KM. RGS16 inhibits breast cancer cell growth by mitigating phosphatidylinositol 3-kinase signaling. J Biol Chem 2009;284:21719–27.
33. Miyoshi N, Ishii H, Sekimoto M, Doki Y, Mori M. RGS16 is a marker for prognosis in colorectal cancer. Ann Surg Oncol 2009;16:3507–14.
34. Hanahan D, Weinberg RA.The hallmarks of cancer. Cell 2000;100:57–70.
35. Nana-Sinkam SP, Croce CM. MicroRNAs as therapeutic targets in cancer. Transl Res 2011;157:216–25.
36. Shah MY, Ferrajoli A, Sood AK, Lopez-Berestein G, Calin GA. microRNA therapeutics in cancer - an emerging concept. EBioMedicine 2016;12: 34–42.
37. Chen Y, Song S, Yan Z, Fenniri H, Webster TJ. Self-assembled rosette nanotubes encapsulate and slowly release dexamethasone. Int J Nanomedicine 2011;6:1035–44.
38. Song S, Chen Y, Yan Z, Fenniri H, Webster TJ. Self-assembled rosette nanotubes for incorporating hydrophobic drugs in physiological environments. Int J Nanomedicine 2011;6:101–7.
39. DiDomenico CD, Bonassar LJ.How can 50 years of solute transport data in articular cartilage inform the design of arthritis therapeutics? Osteoarthritis Cartilage 2018;26:1438–46.
40. DiDomenico CD, Lintz M, Bonassar LJ. Molecular transport in articular cartilage - what have we learned from the past 50 years? Nat Rev Rheumatol 2018;14:393–403.
41. Panyam J, Labhasetwar V. Biodegradable nanoparticles for drug and gene delivery to cells and tissue. Adv Drug Deliv Rev 2003;55:329–47.
42. Prabha S, Zhou WZ, Panyam J, Labhasetwar V. Size-dependency of nanoparticle-mediated gene transfection: studies with fractionated nanoparticles. Int J Pharm 2002;244:105–15.

43. Bharali DJ, Klejbor I, Stachowiak EK, Dutta P, Roy I, Kaur N, et al. Organically modified silica nanoparticles: a nonviral vector for in vivo gene delivery and expression in the brain. Proc Natl Acad Sci U S A 2005; 102:11539–44.
44. Thomas CE, Ehrhardt A, Kay MA. Progress and problems with the use of viral vectors for gene therapy. Nat Rev Genet 2003;4:346–58.
45. Beg MS, Brenner AJ, Sachdev J, Borad M, Kang YK, Stoudemire J, et al. Phase I study of MRX34, a liposomal miR-34a mimic, administered twice weekly in patients with advanced solid tumors. Invest New Drugs 2017;35:180–8.
46. Edgar R, Domrachev M, Lash AE. Gene expression omnibus: NCBI gene expression and hybridization array data repository. Nucleic Acids Res 2002;30:207–10.